

Developments in analysis and design of PET strap MSE walls

R.J. Bathurst, GeoEngineering Centre at Queen's-RMC, Royal Military College, Kingston, Canada

Y. Miyata, Department of Civil and Environmental Engineering, National Defense Academy, Yokosuka, Japan

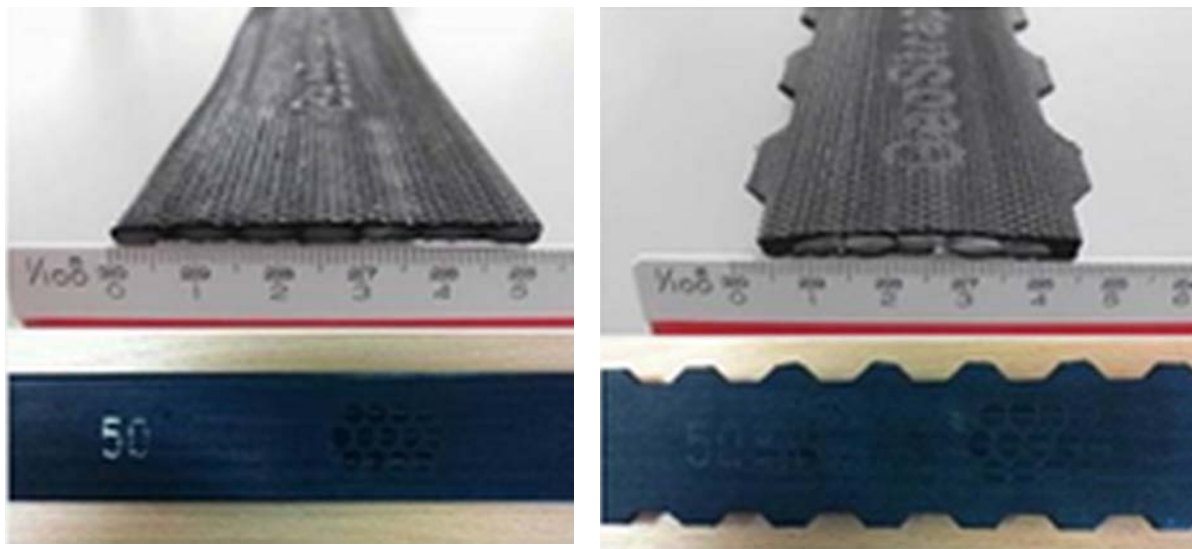
T.M. Allen, Washington State Department of Transportation, State Materials Laboratory, Olympia, Washington, USA

ABSTRACT

Polyester (PET) strap MSE walls are gaining popularity in many countries. The writers compared measured tensile reinforcement loads from instrumented field walls under operational (working stress) conditions with predictions using the Coherent Gravity Method and the Simplified Stiffness Method. These methods are specified in the latest AASHTO code in the USA for MSE walls constructed with inextensible (steel) and extensible geosynthetic reinforcement materials, respectively. Review of the literature shows designers have used the Coherent Gravity Method for PET strap MSE walls in some cases. The paper demonstrates that the Simplified Stiffness Method is accurate for PET strap walls while the Coherent Gravity Method is excessively conservative. The paper reviews the accuracy of candidate pullout models for PET straps. A non-linear pullout model proposed by the writers in an earlier publication is shown to be more accurate than linear and bi-linear models in the AASHTO code specified for other reinforcement materials.

1. INTRODUCTION

Geosynthetic reinforced soil walls constructed with polyester (PET) straps are gaining popularity in many countries. This technology first appeared in the late 1970's (Schlosser et al. 1993) in France, and is described in the French AFNOR (2009) code. However, these walls have only recently appeared in the authoritative AASHTO (2020) LRFD specifications in the USA for geosynthetic reinforced soil walls (called geosynthetic mechanically stabilized earth (MSE) walls in North America). In the AASHTO specifications, PET straps are referred to as "geostrips". At the time of writing, current design codes in Canada, Japan, Hong Kong and the UK remain silent on recommendations for the design of PET strap MSE walls and specifications for the component materials.



a) Single strap with smooth edges

b) Single strap with ribbed edges

Figure 1. Examples of PET strap reinforcement



a) Single strap (Luo et al. 2015)



b) Double strap (Grien and Sankey 2008)

Figure 2. General arrangement for PET strap reinforcement

Figure 1 shows examples of PET strap products. They are typically about 50 to 90 mm wide, 2 to 6 mm thick and comprise of PET fiber bundles encased in a protective polyethylene sheath. They are attached to reinforced concrete panels using steel or HDPE loops cast into the panels. The reinforcement straps are placed in pairs oriented perpendicular to the concrete panels or as a single continuous strap arranged in a splayed pattern (Figure 2).

Table 1 shows an inventory of full-scale instrumented PET strap walls collected by Miyata et al. (2018) that were used to investigate the accuracy of different design methods to predict tensile loads by comparing calculated loads to measured loads deduced from instrumented straps.

Table 1: Summary of instrumented field PET strap MSE walls (from Miyata et al. 2018)

| Wall designation | Construction date | Wall name | Height, H (m) |
|------------------|-------------------|--------------------|---------------|
| PSW1 | 1992 | St. Remy (France) | 6.4 |
| PSW2 | 1991 | Yamaguchi (Japan) | 6.4 |
| PSW3 | 2012 | Delaware (USA) | 8.5 |
| PSW4 (SW) | 2011 | Sao Paulo (Brazil) | 6.4 |
| PSW4 (SP) | | 6.4 | |
| PSW5 | 2013 | Shizuoka (Japan) | 9.6 |
| PSW6 | 2015 | Nagasaki (Japan) | 6.6 |
| PSW7 | 2015 | NIED (Japan) | 6.0 |
| PSW8 | 1995 | Saga (Japan) | 5.6 |

A review of the literature by Miyata et al. (2018) revealed that PET strap walls have been designed according to variants of the Coherent Gravity Method (e.g., AASHTO 2020; AFNOR 2009; BSI 2010; PWRC 2014), that were developed for relatively inextensible steel reinforced soil walls. Other walls were designed using the Simplified Method (e.g., AASHTO 2017, CSA 2019) and variants that were developed for walls constructed with relatively extensible polymeric reinforcement materials (geotextiles and geogrids). Different design methods can be expected to give different maximum tensile loads in the PET strap reinforcement layers under operational conditions.

At the time of writing, the Simplified Stiffness Method (Allen and Bathurst 2015, 2018) has been recently adopted in the AASHTO (2020) LRFD specifications as the primary method for the calculation of maximum tensile loads in geosynthetic reinforced soil walls constructed with geogrids, geotextiles and PET straps (geostrips). In the current AASHTO code the method name is shortened to the "Stiffness Method".

The Coherent Gravity Method appears in the same code for MSE walls and is recommended for MSE walls constructed with relatively inextensible steel strip and steel grid materials. The Coherent Gravity Method has been used by some designers in the past to design PET strap MSE walls as noted by Miyata et al. (2018).

The objective of this paper is to:

- 1) Examine the accuracy of these two load methods for the calculation of the maximum tensile load (T_{max}) in PET strap reinforcement layers by comparing predicted to measured reinforcement loads under operational conditions.
- 2) Examine the accuracy of PET strap pullout capacity models using a database of pullout box tests collected by the writers (Miyata et al. 2019).

2. REINFORCEMENT TENSILE LOADS

2.1 Coherent Gravity Method

The maximum reinforcement load using the Coherent Gravity Method is computed as:

$$T_{max} = S_v \left[K \frac{\sigma_v L}{L - 2e} \right] \quad [1]$$

Here, S_v = tributary vertical spacing of the reinforcement layer; $\sigma_v = \gamma z + q$ = vertical earth pressure at the reinforcement depth z below the wall crest due to soil unit weight γ plus the contribution of uniform distributed surcharge pressure q (Figure 3b); L = reinforcement length at the location of the layer; e = eccentricity due to the retained soil acting against the reinforced soil zone; K = lateral earth pressure coefficient. K varies linearly with depth below the top of the internal soil wedge from $K_0 = 1 - \sin\phi$ to the active earth pressure value $K_a = (1 - \sin\phi)/(1 + \sin\phi)$ at a depth of 6 m, and remains constant thereafter (Figure 3a).

Any cohesive soil strength component is ignored in the calculation of T_{max} . Following the AASHTO interpretation of the Coherent Gravity Method, the peak friction angle of the reinforced soil is capped at $\phi \leq 40^\circ$.

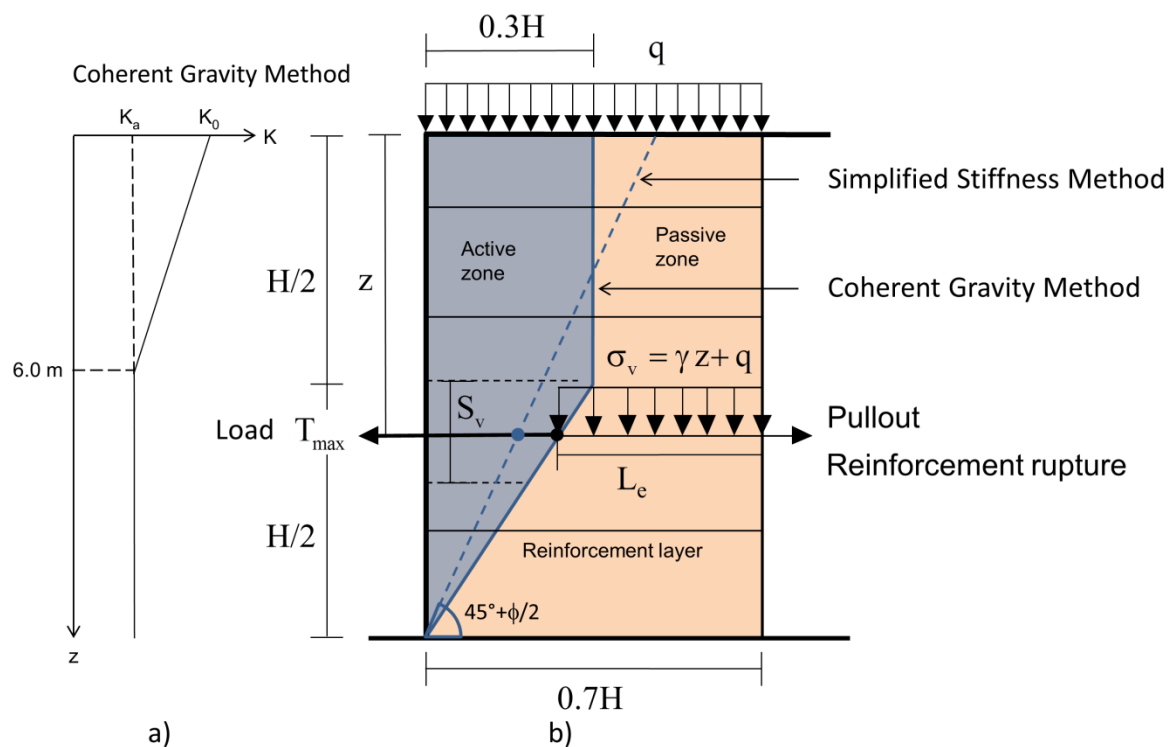


Figure 3. a) Selection of K value for Coherent Gravity Method for case of horizontal back slope, and b) Active- and passive zones for Coherent Gravity Method and Simplified Stiffness Method pullout limit state calculations (AASHTO 2020)

2.2 Simplified Stiffness Method

For vertical face PET strap MSE walls constructed with cohesionless backfill soil and the same reinforcement material placed at the same spacing (constant S_v), the maximum tensile load in a reinforcement layer, T_{max} , using the Simplified Stiffness Method is:

$$T_{max} = S_v \gamma \left[HD_{tmax} + \left(\frac{H_{ref}}{H} \right) S \right] K_a \Phi_g \Phi_{fs} \quad [2]$$

Here, H = wall height; H_{ref} = reference height = 6 m; D_{tmax} = T_{max} distribution factor with depth z below the crest of the wall; S = equivalent height of uniformly distributed surcharge pressure = q/γ ; Φ_g = global (reinforcement) stiffness factor (dimensionless); Φ_{fs} = facing stiffness factor (dimensionless); and other variables have been defined previously. An expanded form of Equation 2 to account for $c-\phi$ soils, inclined wall facings, more than one reinforcement type, and different reinforcement spacing can be found in AASHTO (2020) and Allen and Bathurst (2015, 2018).

Figure 4 shows example curves for distribution factor D_{tmax} . The parameter T_{mxmx} is the maximum reinforcement load from all reinforcement loads in the wall and is located in the bottom half of the wall. A notable feature of the D_{tmax} curves that are computed for geosynthetic MSE walls are the near-bilinear shape. This trend reflects the observation that measured reinforcement tensile loads do not increase linearly with depth below the crest of the wall as may be expected using classical tie-back wedge methods [e.g., the Simplified Method in AASHTO (2017)]. The normalized breakpoint z_b/H shown in the figure becomes deeper as the height of the wall increases.

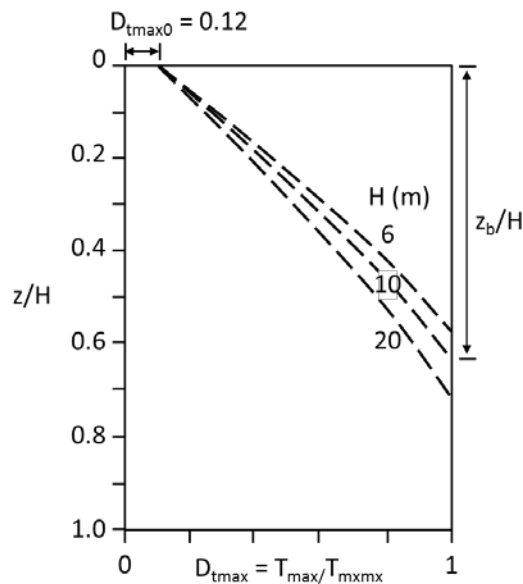


Figure 4. Example T_{max} distribution factors (D_{tmax}) using the Simplified Stiffness Method

An important feature of the Simplified Stiffness Method is the global stiffness factor (Φ_g) which captures the influence of reinforcement stiffness on reinforcement loads under operational conditions and is computed as:

$$\Phi_g = \alpha \left(\frac{S_{global}}{p_a} \right)^\beta \quad [3]$$

Here, S_{global} is the dimensionless global reinforcement stiffness computed as:

$$S_{global} = \frac{1}{H} \sum_{i=1}^m J_i \quad [4]$$

and α and β are constant coefficients equal to 0.16 and 0.26, respectively; J = reinforcement tensile stiffness; m = number of reinforcement layers, and; p_a is atmospheric pressure that is used to normalize the stiffness parameter.

The Simplified Stiffness Method for geosynthetic sheet reinforcement materials (geogrids and geotextiles) specifies that the secant stiffness value J be computed from the 1000-h isochronous creep curve at 2% strain (AASHTO 2020). Miyata et al. (2018) recommended that the stiffness be computed at 1% strain on the same 1000-h curve to capture the lower strains observed in PET strap walls compared to the strains observed for comparable MSE walls constructed with geosynthetic sheet materials (e.g., geogrids and geotextiles). Finally, like the Coherent Gravity Method, AASHTO (2020) recommends that the peak friction angle of the reinforced soil be capped at $\phi \leq 40^\circ$ when using the Simplified Stiffness Method.

The reader is directed to the papers by Allen and Bathurst (2015, 2018) for additional details of the Simplified Stiffness Method and its development.

3. INEXTENSIBLE VERSUS EXTENSIBLE REINFORCEMENT

As noted in the introduction of this paper, PET strap MSE walls have been designed using the Coherent Gravity Method (i.e., assumed to behave as relatively inextensible steel reinforced soil walls) and also as extensible geosynthetic MSE walls (Miyata et al. 2018). The Simplified Stiffness Method is seamless across walls constructed with either reinforcement type when used to compute reinforcement loads under operational conditions. It can also be used to distinguish between these two categories of MSE wall on the basis of wall stiffness quantified by parameter S_{global} as shown in Figure 5.

Figure 5 shows back-calculated values of global reinforcement stiffness factor (Φ_g) from loads deduced from instrumented reinforcement layers in MSE walls (Table 1). The data are parsed into groups based on walls constructed with geogrids and geotextiles, steel strips and steel grids, and PET straps. This calculation was done by isolating Φ_g in the expanded (full) version of Equation 2 and substituting measured values of T_{max} in the formulation.

The data show two distinct groups identified as inextensible ($S_{global} \geq 20$ MPa) and extensible ($S_{global} \leq 2$ MPa). With the exception of the St. Remy wall, the PET strap walls fall in the extensible range with geotextile and geogrids, albeit at the high stiffness end. The St. Remy wall data can be explained by the unusually thick and stiff product used in this early wall compared to the products in the other instrumented structures listed in Table 1 and products used today. Nevertheless, the average value of T_{max} for this wall falls closely on the curve for Φ_g using the Simplified Stiffness Method which points to the utility of the general approach.

The conclusion from the interpretation of data in Figure 5 is that the reinforcement loads for PET strap walls are best computed assuming that the walls behave as extensible geosynthetic reinforced soil walls using the Simplified Stiffness Method. This recommendation has been adopted in the recent AASHTO (2020) specifications.

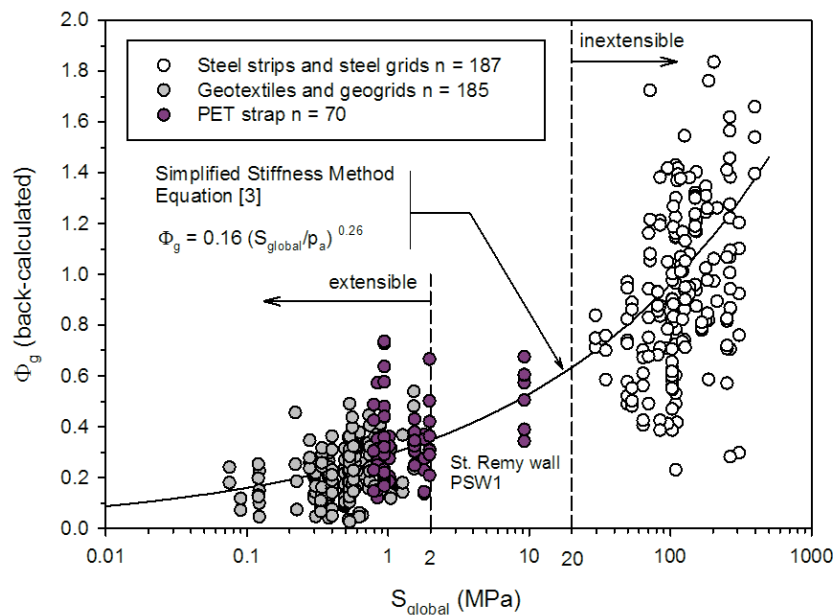


Figure 5. Global reinforcement stiffness factor (Φ_g) versus global reinforcement stiffness (S_{global}) (after Miyata et al. 2018)

4. MEASURED AND PREDICTED TENSILE LOADS

Figure 6 shows predicted tensile loads and measured loads from selected instrumented field walls in Table 1. The predicted loads are computed using the current AASHTO Coherent Gravity Method and the Simplified Stiffness Method described earlier. The plots show that the Simplified Stiffness Method is more accurate than the Coherent Gravity Method, and the Coherent Gravity Method is excessively conservative for design. Similar plots for the other walls in Table 1 are available in the paper by Miyata et al. (2018) and demonstrate the same relative performance described here.

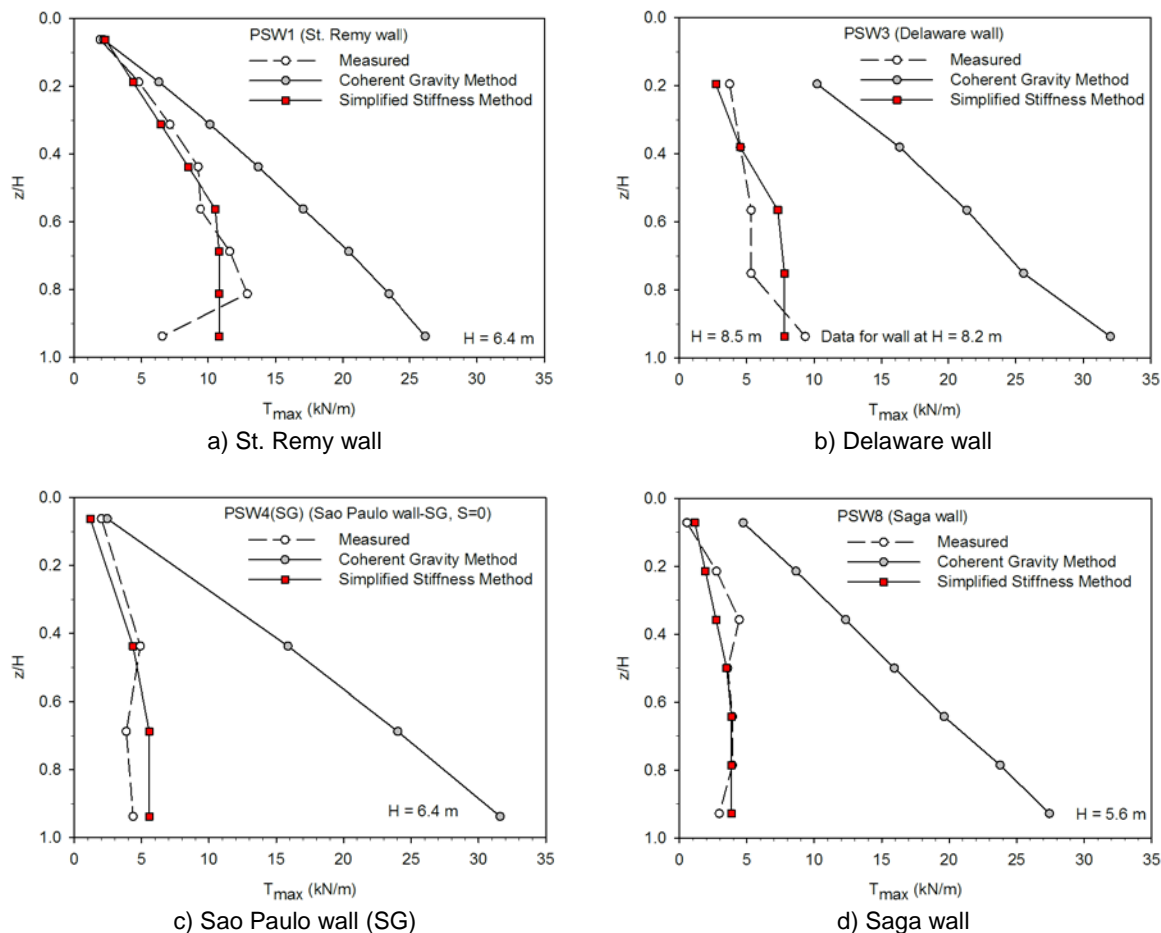


Figure 6. Predicted and measured maximum reinforcement loads (T_{max}) in full-scale instrumented field walls

5. PULLOUT CAPACITY OF SINGLE AND PARALLEL DOUBLE PET STRAPS

Miyata et al. (2019) investigated the accuracy of linear models used for geosynthetics, and bi-linear pullout models that are used for steel strips, by comparing predicted pullout capacities with measured values from laboratory pullout box tests on PET straps. An improved model of non-linear form was also investigated. The three types of models were investigated for single strap and parallel double strap configurations. Due to limited space only three permutations for single straps are reported here. The general expression for ultimate pullout capacity (P_c) in units of force per unit running length of wall (e.g., kN/m) is:

$$P_c = F^* \sigma_v L_e b_w \quad [5]$$

The difference between models is captured by the dimensionless interaction coefficient F^* . The general form of F^* is shown in Figure 7. Parameter σ_v = normal pressure acting at the elevation of the reinforcement (as before), L_e = length of the reinforcement in the passive soil zone (Figure 3b), and b_w = the effective width of the PET strap element (i.e., one strap or outside width of double straps).

The first category comprises of linear equations where F^* is constant with depth z (Figure 7a). The example used here is:

$$F^* = f_0 = f_1 = 0.67 \tan \phi \quad [6]$$

This is the default equation in AASHTO (2020) for geogrids and geotextiles. The second category of pullout equations describes F^* as a bi-linear function of depth z , as shown in Figure 7b. Hence, coefficient F^* can be expressed as:

$$F^* = f_0 (1 - z/z_0) + f_1 (z/z_0) \quad \text{for } z \leq z_0 = 6 \text{ m} \quad [7a]$$

$$F^* = f_1 \quad \text{for } z > z_0 = 6 \text{ m} \quad [7b]$$

In AASHTO (2020) specifications for ribbed steel strips, $f_0 = 1.2 + \text{Log}U_c$ (where U_c is the coefficient of uniformity of the granular soil) and f_0 is capped at 2, and $f_1 = \tan \phi$. The third category of pullout equations in this paper has been proposed by Miyata et al. (2019) and has exponential form as illustrated in Figure 7c. An exponential expression of this type has also been proposed by Miyata and Bathurst (2012) for steel strips. In the current study it is written as:

$$F^* = f_1 + \frac{f_0 - f_1}{\exp\left(c \frac{\sigma_v}{p_a}\right)} \quad [8]$$

In this paper we use the following parameter values: $f_0 = 1.5$, $f_1 = 0.5$ and $c = 2.3$. Atmospheric pressure $p_a = 101 \text{ kPa}$ is used to normalize the vertical stress term; for $\sigma_v \rightarrow \infty$ (i.e., increasing z), $F^* \rightarrow f_1$. This equation has the same number of coefficients (i.e., fixed values) as Equation 7, but has the advantage of being smoothly continuous.

In the remainder of this section the accuracy of the three models with single strap configurations is quantified using analysis of bias statistics where bias is the ratio of measured pullout capacity divided by predicted value. A model is judged to improve as the mean of bias values approaches one, the coefficient of variation (COV) of bias values is small, and bias dependencies (i.e., correlations) with vertical stress and predicted values of P_c are small or negligible at a level of significance of (say) 5%. Plots of measured versus predicted pullout capacity are shown in Figures 8a, 9a and 10a. The data are plotted with logarithmic axes to avoid visual clutter at low pullout capacity values. The data in Figure 8a mostly fall above the one to one correspondence line demonstrating that the model is conservative. The corresponding mean bias value is 1.44, meaning that measured pullout capacities are 44% higher than predicted values “on average”. Thus the model error is on the safe side for design. The spread in bias values (COV) is 28%. The same model shows that bias values are strongly correlated with predicted pullout capacity (Figure 8b) and normal stress (Figure 8c). This demonstrates that the accuracy of the pullout model varies with magnitude of the predicted pullout capacity and normal stress level. This is an undesirable feature of this model.

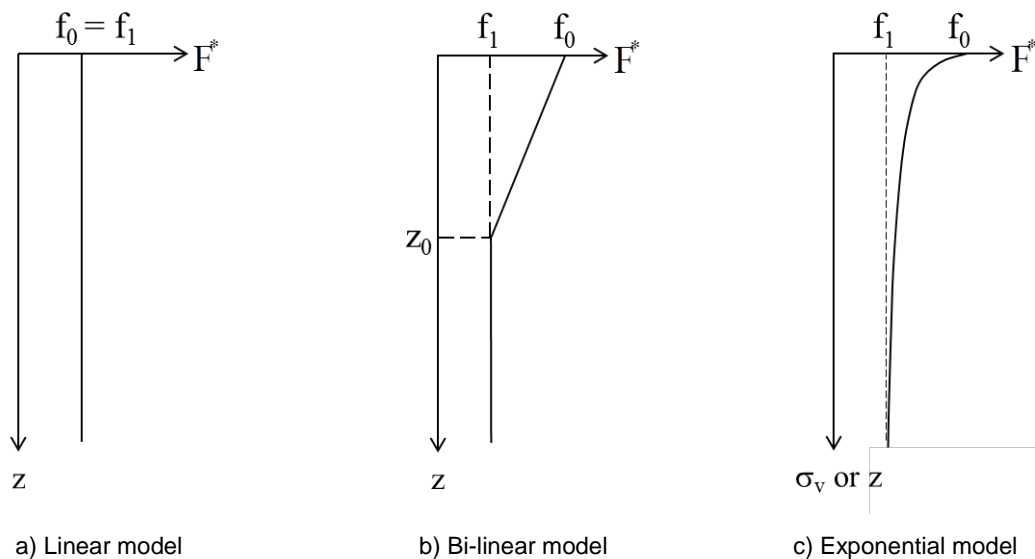
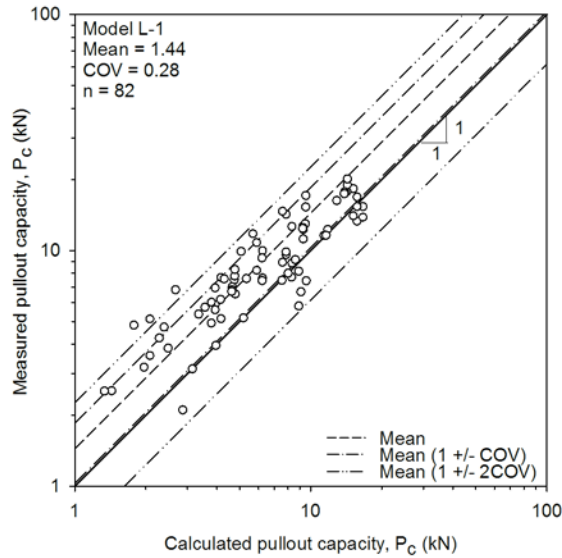
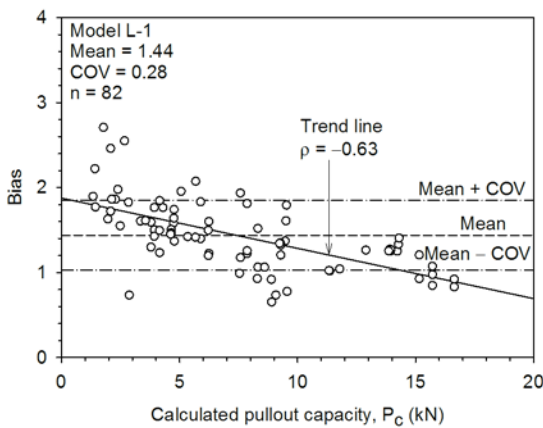


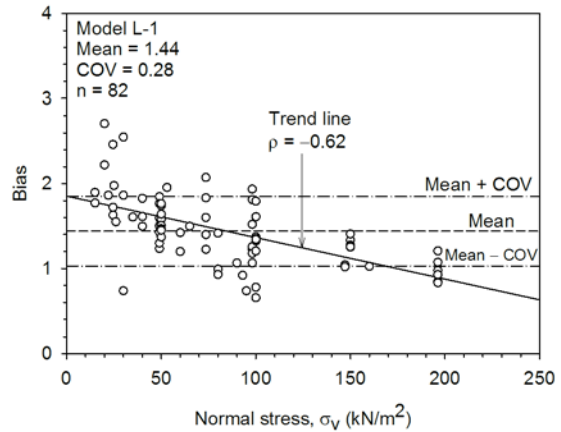
Figure 7. Interaction coefficient F^* functions for different pullout models



a) Measured versus calculated pullout capacity



b) Bias versus calculated pullout capacity



c) Bias versus normal stress

Figure 8. AASHTO (2020) linear pullout model for single straps (after Miyata et al. 2019)

Correlations with predicted pullout capacity and vertical stress are very much less using the AASHTO bi-linear model (Figures 9b and 9c). However, this model typically overestimates the measured pullout capacity by what is judged to be a large margin (Figure 9a). The mean bias value of 0.70 indicates that the measured values are only 70% of the predicted values on average, which is non-conservative for design. The accuracy of the model with respect to the spread in bias values (COV = 0.25) remains about the same as the linear model (COV = 0.28).

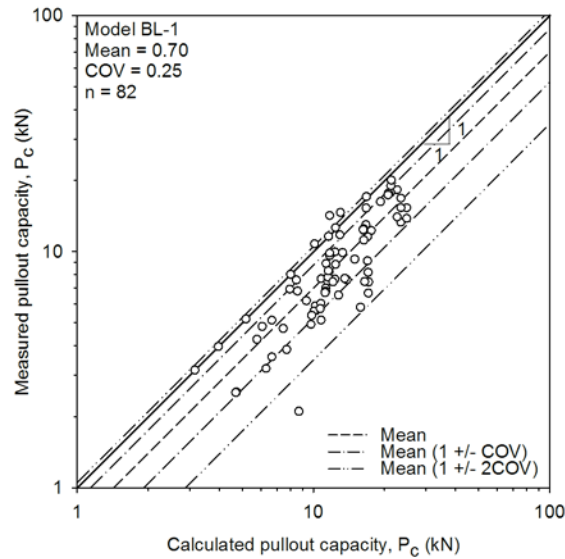
The plots in Figure 10 and the computed bias statistics show that the non-linear model is more accurate on average, and undesirable dependencies noted earlier are no longer present.

6. CONCLUSIONS

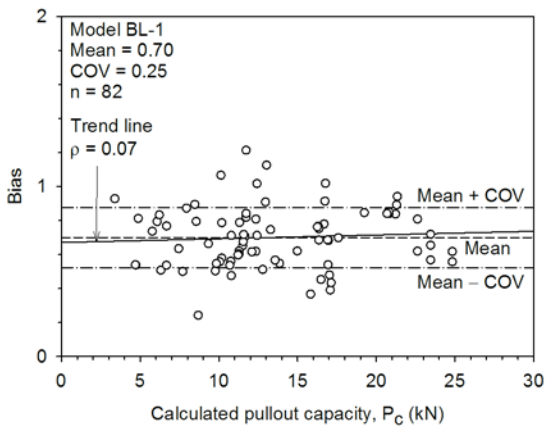
This paper has reviewed recent work by the writers focused on the assessment of load and pullout models for the internal stability design of PET strap MSE walls.

This paper shows that the Coherent Gravity Method that has been used by some designers is not appropriate and is excessively conservative for internal stability design of PET strap MSE walls. The recently adopted Simplified Stiffness Method that is specified in the latest AASHTO code in the USA as the primary design method for geosynthetic MSE walls, is more accurate.

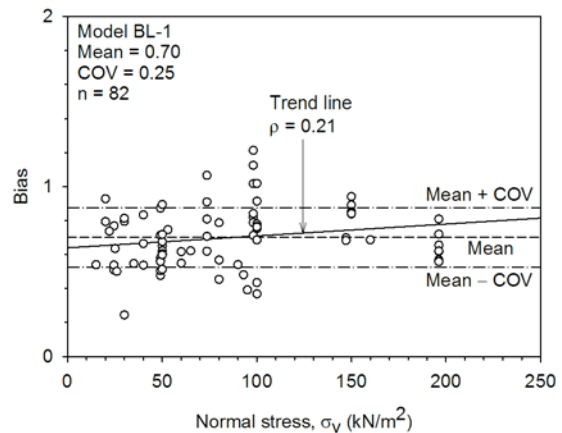
The paper also reviews the accuracy of candidate pullout models for PET strap MSE walls. This review shows that a non-linear pullout model proposed by the writers in an earlier publication is more accurate than linear and bi-linear models that have been used for other reinforcement materials in the current AASHTO code.



a) Measured versus calculated pullout capacity



b) Bias versus calculated pullout capacity



c) Bias versus normal stress

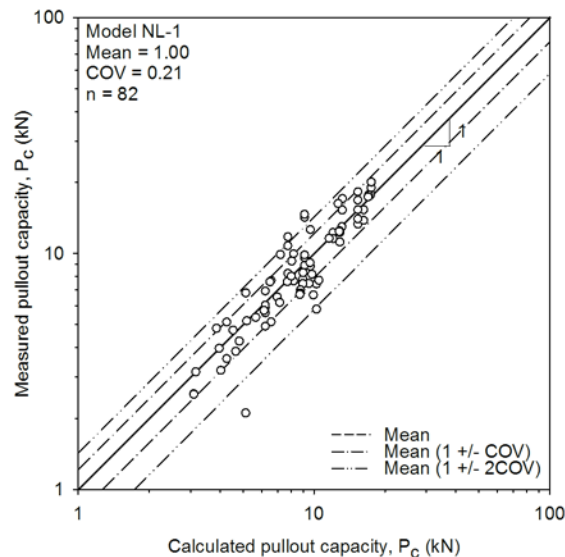
Figure 9. AASHTO (2020) bi-linear pullout model for single straps (after Miyata et al. 2019)

Readers are directed to the publications by Miyata et al. (2018, 2019) for additional examples and a deeper treatment of the two subject areas discussed in this paper.

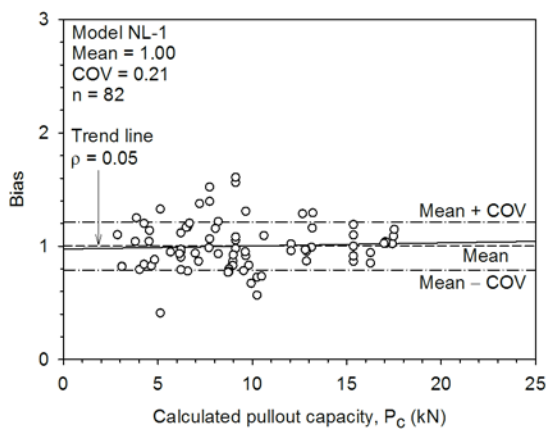
REFERENCES

- Allen, T.M. and Bathurst, R.J. (2015). An improved simplified method for prediction of loads in reinforced soil walls. *Journal of Geotechnical and Geoenvironmental Engineering* 141(11): 04015049.
- Allen, T.M. and Bathurst, R.J. (2018). Application of the Simplified Stiffness Method to design of reinforced soil walls. *Journal of Geotechnical and Geoenvironmental Engineering* 144(5): 04018024.
- AFNOR (2009). NF P94-270: Renforcement des sols. Ouvrages en sol rapporté renforcé par armatures ou nappes extensibles et souples. Dimensionnement (Association Française de Normalisation). La Plaine Saint Denis cedex – France. (in French)
- AASHTO. (2017). LRFD Bridge Design Specifications, 8th Ed., American Association of State Highway and Transportation Officials (AASHTO), Washington, DC, USA.
- AASHTO. (2020). LRFD Bridge Design Specifications, 9th Ed., American Association of State Highway and Transportation Officials (AASHTO), Washington, DC, USA. (in press).
- British Standards Institution (BSI). (2010). BS8006-1:2010+A1:2016: code of practice for strengthened/reinforced soil and other fills. British Standards Institution, Milton Keynes, UK.

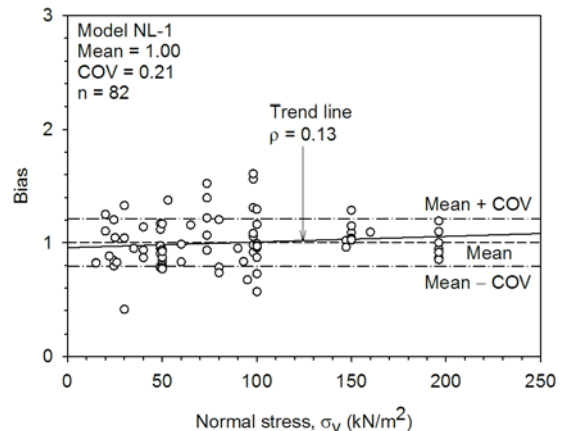
- CSA. (2019). Canadian Highway Bridge Design Code. CAN/CSA-S6-19. Canadian Standards Association (CSA), Mississauga, Ontario, Canada.
- Grien, M.J. and Sankey, J.E. (2008). High capacity geostrap reinforcement for MSE structures. Proceedings of 5th International Symposium on Earth Reinforcement, Fukuoka, Japan. pp. 503-506.
- Luo, Y., Leshchinsky, D., Rimoldi, P., Lugli, G. and Xu, C. (2015). Instrumented mechanically stabilized earth wall reinforced with polyester straps. Transportation Research Record, 2511, 9-17.
- Miyata, Y. and Bathurst, R.J. (2012). Analysis and calibration of default steel strip pullout models used in Japan. Soils and Foundations 52(3): 481-497.
- Miyata, Y., Bathurst, R.J. and Allen, T.M. (2018). Evaluation of tensile load model accuracy for PET strap MSE walls. Geosynthetics International 25(6): 656-671.
- Miyata, Y., Bathurst, R.J. and Allen, T.M. (2019). Calibration of PET strap pullout models using a statistical approach. Geosynthetics International 26(4): 413-427.
- Public Works Research Center (PWRC). (2014). Design Method, Construction Manual and Specifications for Steel Strip Reinforced Retaining Walls (4th Ed.). Public Works Research Center, Tsukuba, Ibaraki, Japan, 477 p. (in Japanese)
- Schlosser, F., Hoteit, N. and Price, D. (1993). Instrumented full scale Freyssisol-Websol reinforced wall. Proceedings of Soil Reinforcement: Full Scale Experiments of the 80s, ISSMFE/ENPC, Paris, France, pp. 299-320.



a) Measured versus calculated pullout capacity



b) Bias versus calculated pullout capacity



c) Bias versus normal stress

Figure 10. Non-linear pullout model for single straps (after Miyata et al. 2019)